crystals

MDPI

Article

Plasmonic Photomobile Polymer Films

Riccardo Castagna [1,*], Massimo Rippa [1], Francesco Simoni [1,2,*], Fulvia Villani [3], Giuseppe Nenna [3] and Lucia Petti [1]

1 Institute of Applied Sciences and Intelligent Systems, CNR, 80078 Pozzuoli (Napoli), Italy; massimo.rippa@isasi.cnr.it (M.R.); lucia.petti@isasi.cnr.it (L.P.)
2 Dipartimento SIMAU, Università Politecnica delle Marche, 60131 Ancona, Italy
3 Nanomaterials and Devices Laboratory, ENEA, 80055 Portici (Napoli), Italy; fulvia.villani@enea.it (F.V.); giuseppe.nenna@enea.it (G.N.)
* Correspondence: riccardo.castagna@isasi.cnr.it (R.C.); f.simoni@univpm.it (F.S.)

Received: 10 June 2020; Accepted: 17 July 2020; Published: 1 August 2020

Abstract: In this work, we introduce the approaches currently followed to realize photomobile polymer films and remark on the main features of the system based on a biphasic structure recently proposed. We describe a method of making a plasmonic nanostructure on the surface of photomobile films. The characterization of the photomobile film is performed by means of Dark Field Microscopy (DFM), Scanning Electron Microscopy (SEM), and Atomic Force Microscopy (AFM). Preliminary observations of the light-induced effects on the Localized Surface Plasmon Resonance are also reported.

Keywords: plasmonics; photomobile polymer films; localized surface plasmonic resonance; flexible substrates

1. Introduction

The direct conversion of light into mechanical work [1,2] could play an important role in harvesting energy [3,4], allowing further development of the sector by giving different alternatives to the energy storage [5]; at the same time, the light-induced actuation of the material would be able to add additional properties to previously fabricated nanostructures. In particular, it would be of great interest to have nanostructures with plasmonic properties that can be modulated by photoactuation.

To this aim, different scientific problems linked to two different technologies have to be solved. One concerns the approach chosen to obtain a photomobile film, and the other concerns how to associate the nanostructure to it.

It is well known that different solutions have been proposed to get photo-induced actuation. In the recent decade, Marangoni's effect [6] induced by light has been proposed as a basic mechanism to induce and control the motion of macro- or micro-objects floating on a liquid surface [7–10]. Its working mechanism is based on the surface tension gradient induced by light close to the object that should be moved. Photochromic capillary effects are also widely reported and studied [11,12]. However, the most popular way to obtain the direct conversion of light into mechanical work is based on the use of a particular kind of liquid crystalline polymer with the inclusion of azobenzenes moieties. The first realization of such a compound has to be attributed to Angeloni et al. [13], while the realization of very efficient acrylate azobenzene-based photomobile polymer (PMP) films was reported for the first time by Ikeda's group [2]. These materials allow the direct conversion of light energy into mechanical work: the PMP film bends under the illumination of light with the specific characteristics and bending efficiency dependent on the intensity, polarization, and wavelength of the incident light.

In this case, the mechanism responsible for the light-induced bending of azo-benzene-based liquid crystal PMP films (azo-LC-PMP) is the *cis-trans* photo-isomerizations leading to the film deformation at a macroscopic level, while the liquid crystal configuration of the system allows the alignment of

the molecules containing the azo-benzene groups during the thermally induced polymerization that brings formation to the film. Since photo-isomerization is strongly dependent on the wavelength and on the polarization state of the incident light, the same dependence is found in the bending process.

The different properties obtained with different compounds in the last decades are substantially based on the different lengths of the alkyl chains of the monomers forming the final polymer film. In short, two monomers are present in the system: one with the azobenzene moiety linked to two acrylate functions, while the other one has the azobenzene moiety linked to one acrylate functional group.

The consequence of the photo-isomerization of all the components of the film is the light-induced bending. UV-light is used to get *cis-trans* isomerization leading to bending, while visible light induces the opposite process, allowing a quick recovery of the initial condition.

A further development brought to the realization of azo-LC-PMP is its ability to oscillate under continuous illumination at a frequency of up to about 26 Hz with a lifetime of about 2.5 h, as reported by White et al. in 2008 [14]. These materials are very interesting because of the large bending angle and pretty high oscillation frequency induced by light under different conditions of wavelengths and polarization states. In order to be active, these materials require a pre-exposure step using a specific light polarization necessary to align the molecules in the system.

In general, the molecular structure of polymers suitable for realizing PMPs should be mainly based on linear or ramified chains, but never reticulated ones. This is a typical feature of thermoplastic materials where the polymer chains are linked together through secondary bonds (van der Waals forces and hydrogen bridge bonds) that can be easily broken by mechanical, thermal, or photothermal (in this case) excitation [15].

Recently, a new approach has been proposed for the realization of PMP films based on a biphasic architecture [16]. This configuration can be considered as an emerging novel research direction for the fabrication of efficient PMPs. The actuation mechanism is based on the difference in expansion coefficients (under illumination) of the two polymeric layers, resulting in the bending of the PMP film. In this case, there is no need of an additional light beam to restore the initial position of the film: when the light is switched on, the film bends; when the light is switched off, the film goes back to its initial condition. Since this approach has been chosen to obtain a polymeric film with plasmonic properties, we will briefly review its properties in the next section.

Concerning the realization of nanostructures with plasmonic properties, different patterning techniques have been developed; however, the most popular and efficient one is based on Electron Beam Lithography (EBL). It allows fabricating high-quality nanostructures using different geometries, realizing large area 2D crystals, which are often called "plasmonic crystals", when plasmon resonance is achieved by the proper choice of materials (usually gold on silica glass), the shape of the nanoelements, and the crystal lattice.

Among the few examples where an ordered structure, i.e., a 2D crystal made by micropillars/microwells, is modified by the action of light, we remind of the one recently reported by Pirani et al. [17,18]. In addition in this case, the photo-isomerization of azobenzene moieties is exploited. Nevertheless, this structure did not include plasmonic properties.

On the other hand, the realization of PMP films that are able to host plasmonic crystals is a real challenge for Material Science. In the past two decades, advanced technologies based on plasmonics have been developed such as Localized Surface Plasmonic Resonance (LSPR) [19–21] and Surface Enhanced Raman Scattering (SERS) [22–26] allowing the detection of monomolecular layers and measurements of refractive index changes at the nanoscale. The implementation of these techniques is usually obtained by realizing metallic nano-elements (nanopillars or nanocavities) on rigid substrates [27,28]. The fabrication of these structures on flexible supports might provide new potential applications for these technologies (e.g., by adapting plasmonic devices for topical investigations) [29,30]. Some advances in this field are represented by plasmonics structures realized on flexible and extensible soft polymers used for molding and the transfer of previously realized nanopatterns [31–34].

However, the realization of a plasmonic nanostructure on a photomobile polymeric surface has not been reported yet, which is probably because those structures are realized by a lithographic process that requires solvents (developers and removers), critically affecting their implantation on PMP films.

The aim of the present work is to give a demonstration that by using our unconventional approach for the realization of a photomobile polymer film, it is possible to transfer on it a gold nanostructure that keeps its plasmonic properties; then, it is possible to realize a plasmonic PMP film. In the next section, we briefly review the properties of the photomobile material before describing the focus and the achievements of this research in Section 3.

2. A New Approach: Modulation of the Surface Tension at a Biphasic Interface

We have recently proposed a novel, fast, and inexpensive approach to processing PMP films [16]. In this case, PMP is obtained by the photopolymerization of an organic mixture sandwiched between two slide glasses. The mixture components have different polymerization rates; they are di-pentaerythritol-penta/hexa-acrylate (DPEPA), 1-vinyl-2-pyrrolidinone (NVP), and 4-aminophenol (4-AP) (Sigma-Aldrich, St. Louis, MO, USA). Bis (2,4,6-trimethylbenzoyl) phosphines (CIBA, Basel, Switzerland) is used as a photoinitiator. Details are reported in Castagna et al. [16]. In short, an 8:1 molar ratio of NVP to DPEPA and illumination by one side of the sample allows getting an asymmetric photopolymerization process; therefore, the fabricated film results in a flexible system that is composed by a harder DPEPA-co-NVP network and a softer doped-NVP part, in which a presence of oligomers is identified. The Scanning Electron Microscopy (SEM) (Raith 150, Dortmund, Germany) images show a brush-like morphology in the DPEPA-co-NVP side, when dissolving the film in N-methyl-pirrolidinone (Sigma-Aldrich, St. Louis, MO, USA); while a viscous component is on the other side of the film. The basic film structure can be seen as made by two different inter-digitized parts: one more rigid, but flexible, (the reticulated one) acting as a sort of supporting skeleton for the system, while the second acts as the effective light-activated motor of the system. The phase separation process, occurring in the bulk during photopolymerization, is responsible for the observed bristles structure. Actually, the resulting observed morphology is reminiscent of the one obtained by phase separation in holographic polymer dispersed liquid crystals (HPDLCs), where an alternating sequence of liquid crystal-rich and polymer-rich regions is obtained [35–37]. Here, soft doped-NVP plays the same role of inert LC in HPDLCs. Thus, in our case, as mentioned, the doped-NVP-richer part is the actual motor of the PMP film.

Some preliminary observations [16] suggested that 4-AP-doped NVP could act as a driving motor for the light-induced motion of a composite film when included in the PMP mixture, as a result of the light-induced changes of the surface tension at the interface between the DPEPA skeleton and the NVP-rich side. The reduction of surface tension gradient increases the tendency of NVP to escape when illuminated by light. As a consequence, the thin highly reticulated film of DPEPA tends to bend. By using in place of NVP a different similar compound—for instance, N-methyl-pyrrolidinone (NMP), which has a structure similar to NVP, but does not allow the formation of oligomers/polymers—no movement is observed under illumination, underlining the need to include NVP in the system.

Switching-off the incident beam results in restoring the original shape of the material and, as a consequence, of the whole PMP film. In this way, the viscoelastic properties of the 4-AP-doped NVP together with the re-adaptation of the harder polymeric network of DPEPA brings the film to the original position. The working mechanism of the described PMP film is depicted in Figure 1, in which the initial position (Figure 1a) is obtained when the light is switched-off, while the bending (Figure 1b) under light illumination.

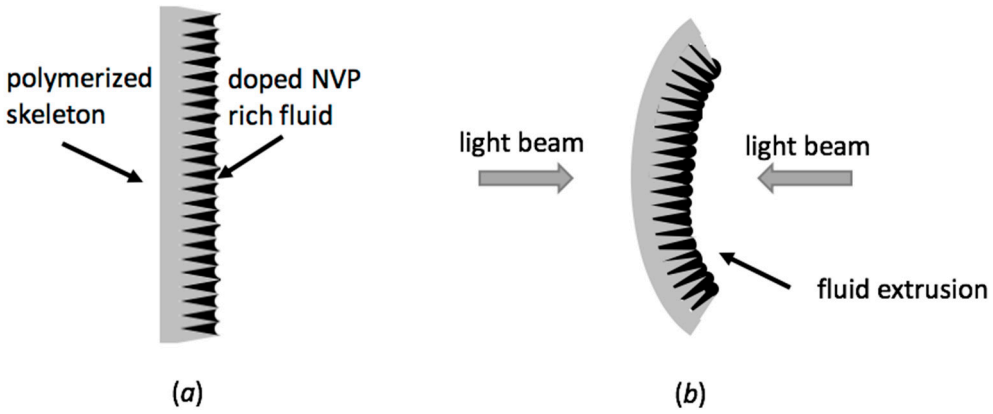

Figure 1. Sketch of the working mechanism of photomobile polymer (PMP) based on di-pentaerythritol-penta/hexa-acrylate (DPEPA)-co-NVP (1-vinyl-2-pyrrolidinone) film: (**a**) before light irradiation; (**b**) under light irradiation (from either side of the film).

The demonstration of the photomobile properties of this film has been given in a simple experiment reported by Castagna et al. [16]. It is remarkable that the bending direction of the polymeric stripe is not dependent on the illumination side (Figure 1b), while the amount and rate of bending increase with the light intensity and depend on the used wavelength.

The advantages of this approach over the other methods to realize PMPs relies on the very easy and extremely cheap way to obtain these films. As a matter of fact, the PMP film is obtained in one step: the photopolymerization synthesis, using commercially available compounds. Large bending angles are obtained, and the film is easily activated (low energy doses are required to move the film). The drawback is the slow relaxation time (the time required to restore the initial position of the film), being governed by diffusion and capillary forces. At the present state of the art, this prevents the achievement of high oscillation frequencies.

One basic property of the used mixture is a strong shrinking effect under photopolymerization [38–46] with the potential to act as a glue [47–54]. As mentioned, the PMP film is made by a double-layered structure realized by an asymmetric photopolymerization process [16]. As a consequence, the PMP film component with a higher degree of polymerization is the first one interacting with the incoming polymerizing light (as confirmed by Attenuated Total Reflectance/Fourier Transform Infra-Red (ATR/FT-IR) measurements [16]). This is mainly made by the polymerized, highly cross-linked, multi-acrylate present in the mixture. In these conditions, when polymerized, multi-acrylate is able to act as a glue. The polymer shrinkage is well assessed in acrylate/multi-acrylate systems [38–46]: it is due to the conversion of sp2 carbon to carbon double bonds to sp3 carbon–carbon bonds under polymerization. In the first case, the intermolecular distances are in the range of approximately 4–5 Å, while in the second case, they are reduced (C-C bonds length is approximately 1.4 Å). This property makes the material suitable for realizing a plasmonic photomobile film, as described in the next section.

3. Plasmonic Photomobile Films

The basic idea to achieve the goal of realizing a plasmonic nanostructure on a photomobile film is based on exploiting the "glue" property of our PMP film in order to pull up gold from nanopillars-based plasmonic nanostructures. We show that this process, in our experimental conditions, gives rise to a complementary gold nanocavities-based pattern nestled on the surface of the PMP film, as explained in the following.

The nanostructure is previously fabricated on Indium Tin Oxide (ITO)-glass slides by a standard Electron Beam Lithography (EBL) technique onto a polymeric electronic resist followed by gold evaporation [25,26]: due to the lift-off process of the resist, the nanopattern is formed by gold nanopillars on the substrate. The mixture to prepare PMP is made by approximately 65% of mixture

A (composed by NVP (90%) and oxidized-4-AP (10%)), 35% of mixture B (composed by DPEPA (approximately 97%) and Irg819 (approximately 3%)) blended together. The fabrication process of the plasmonic PMP film is sketched in Figure 2. The PMP mixture is placed by capillarity in a sandwich formed by two glass slides separated by 100 µm Mylar spacers. The internal surface of one glass slide is made by the previously fabricated nanostructure based on gold nanopillars through the EBL (steps (1), (2) in Figure 2) as similarly described in previous papers [25,26]. Two types of plasmonic quasi-crystals were fabricated: (1) an octagonal pattern with gold nanopillars with a diameter d = 750 nm and minimum interparticles distance a = 180 nm; and (2) a dodecagonal pattern with gold nanopillars with d = 500 nm and a = 1000 nm. In both structures, the height of the gold nanopillars is approximately 60 nm.

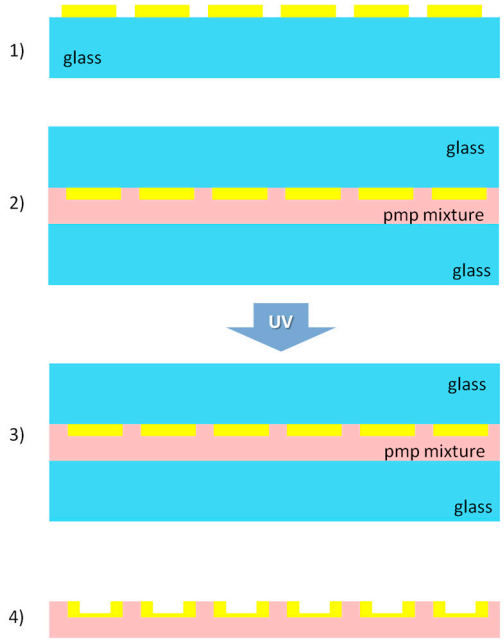

Figure 2. Sketch of the plasmonic photomobile polymer (PMP) fabrication procedure. (**1**) Plasmonic crystal is fabricated on a rigid glass slide substrate (plasmonic crystal on glass slide, PCGS); (**2**) PMP mixture is placed in a sandwich consisting of PCGS and another glass slide separated by mylar spacers; (**3**) ultraviolet irradiation on the PCGS side; (**4**) after irradiation, the PMP film is peeled off from the system, resulting in the plasmonic PMP structure.

Then, step (3) in Figure 2, the photopolymerization is induced by irradiation with a UV-A lamp (Philips TL-D 18W BLB) lasting 40 min. During the illumination, the distance between the lamp and the sample was set at 2 cm. At the end of the process, the sandwich is opened from the non-structured side and left in aerobic conditions for a week. At this stage, the PMP film is easily removable from the glass surface by the use of a cutter. The strong shrinkage of multi-acrylate gives rise to the exfoliation of the gold nanostructures, producing finally the plasmonic PMP.

When the PMP film is peeled-off from the sandwich, step (4) in Figure 2, a reproduction of the nanopattern is obtained on the PMP surface film. This is firstly checked by Dark Field Microscopy (DFM) imaging (see Figure 3, which contains the images of the nanostructure on the rigid substrate (a) and on the PMP film (b). The same pattern can be observed even if the details cannot be seen due to the limited spatial resolution). Details are clear in Figures 4 and 5, reporting data obtained by Scanning Electron Microscopy (SEM) and Atomic Force Microscopy (AFM) (Digital Instruments, Dimension 3100-Nanoscope IV, Veeco, New York, NY, USA). The efficiency of the transfer process of the nano-pattern is investigated by LSPR; in fact, the LSPR peak of the nanopillars on the ITO–glass substrate falls in the red region, having a maximum extinction at λ = 663 nm, while the LSPR peak for the nanostructure on the NPV-based PMP is located at λ approximately 949 nm. This remarkable

shift is due to the difference between the refractive indices of the nanostructures substrate, being the polymer refractive index higher than the ITO glass slide.

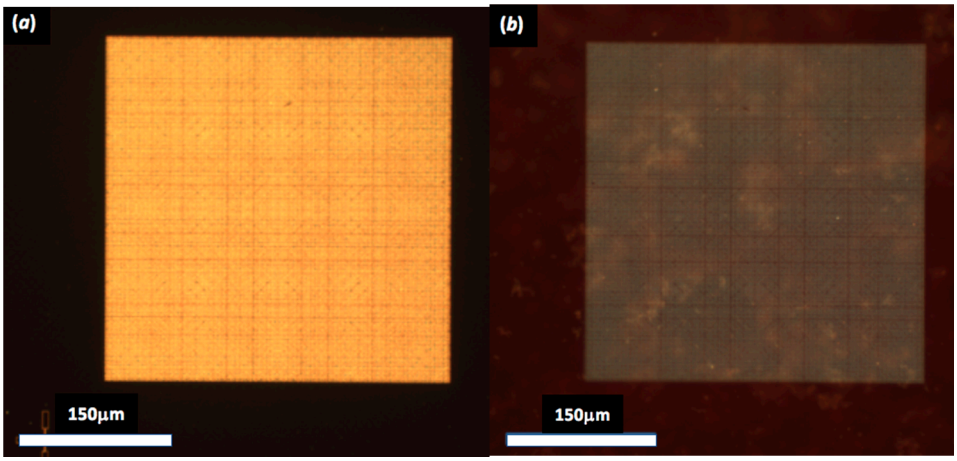

Figure 3. Dark Field Microscopy (DFM) of plasmonic aperiodic crystals (octagonal symmetry) placed: (**a**) on a rigid substrate (glass slide) and (**b**) its complementary nestled on PMP film. Magnification: 20×. The image is collected by an Olympus optical microscope equipped by a Charge Coupled Device CCD camera connected to a computer. The length scale is shown by the white bar (150 μm) at the bottom of the figures.

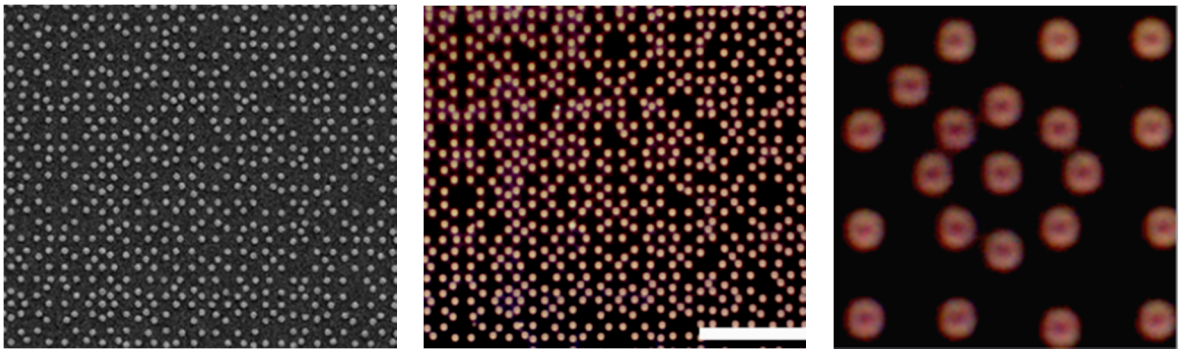

(**a**) (**b**) (**c**)

Figure 4. Comparative analysis of (**a**) octagonal symmetry of plasmonic quasi-crystal on glass (SEM image; columns diameter: approximately 750 nm) and (**b**) the complementary transferred on the surface of the PMP film (DFM; Magnification: 50×). (**c**) Zoom of the structure shown in (**b**).

A comparative analysis between the nanostructures with octagonal symmetry realized on the glass substrate and the ones obtained on the PMP film is performed by DFM and Scanning Electron Microscopy (SEM) and shown in Figures 3 and 4.

By looking at Figure 4, the pattern realized on the solid substrate (see Figure 4a) is exactly reproduced on PMP (Figure 4b). In order to investigate the details of the copy process, it is useful to increase the image magnification, as reported in Figure 4c. We notice the apparent "donut" shape highlighted by the darker part in the center of each single gold element of the pattern. This result points out a refractive index difference between the edge (white) and the center (dark) of the rings that corresponds to a different gold concentration, which is higher at the edges and lower in the center. We can explain this observation taking into account that the roughness on the tip of the pillars does not allow a uniform gold exfoliation.

An additional demonstration of the result of the exfoliation method is shown in Figure 5 where topography (Figure 5a–c) and phase (Figure 5d) measurements obtained by AFM are reported for a plasmonic substrate with dodecagonal symmetry.

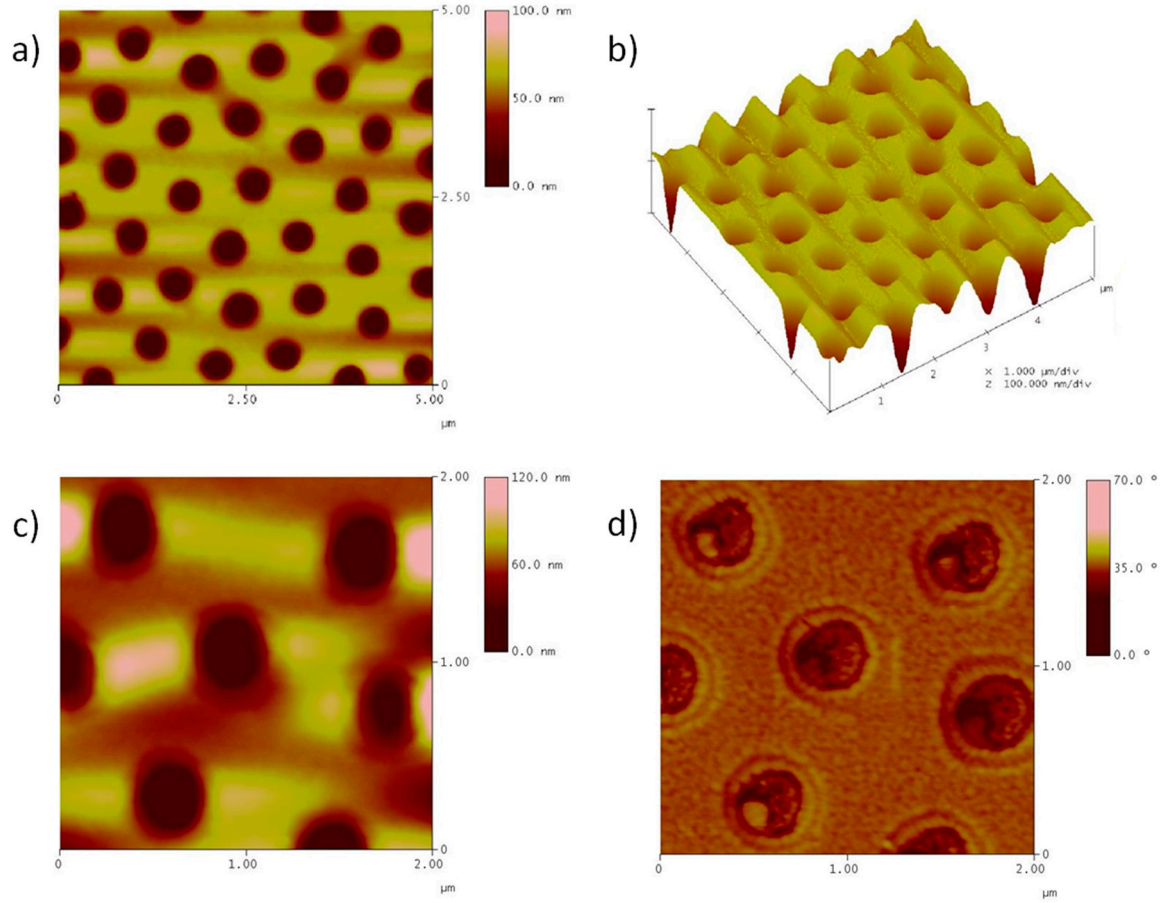

Figure 5. Atomic Force Microscopy (AFM) topography (**a**–**c**) and phase (**d**) images on dodecagonal plasmonic crystals implanted on PMP film. The side of the square image in (**a**,**b**) is 5 µm; in (**c**,**d**), it is 2 µm. The colored bar on the right in (**a**,**c**,**d**) explains the color scale in the images.

All these measurements highlight the following: (1) the good reproduction of the quasi-periodic nanostructure; (2) the presence of nanocavities; (3) the presence of roughness into each single nanocavity; (4) the reproducibility of the method to get any periodic and aperiodic nano-configuration. They are in good agreement with the SEM measurements reported in Figure 4, where the roughness in the center of each single gold nanopillar is evident.

The Localized Surface Plasmon Resonance (LSPR) is strongly dependent on the particular shape of each single nano-element; therefore, we expect the resonance peak of the nanocavity structure to be located in a different position with respect to that of the pillars' structure; moreover, we expected the shape of the resonance to be affected by the PMP substrate.

The measurement of the LSPR peak has been performed using a conventional set-up. A white light of a halogen source (HL 2000-Ocean Optics) is coupled to an Olympus microscope by an optical fiber and focused inside the structure under investigation by an objective (M 40×, NA 0.65) through a diaphragm. The sample is positioned on an XYZ microstage that allows the careful selection of the structure to be investigated. The transmitted signal is collected by an optical fiber with a core of 50 µm and detected using a spectrometer (USB4000-Ocean Optics). A scheme for the set-up is reported in a previous paper [21].

The results of the LSPR measurements are shown in Figure 6. At this stage, we have measured the LSPR peak shift under illumination with a laser pointer (λ = 405 nm; P ~25 mW; spot area ~1 cm^2).

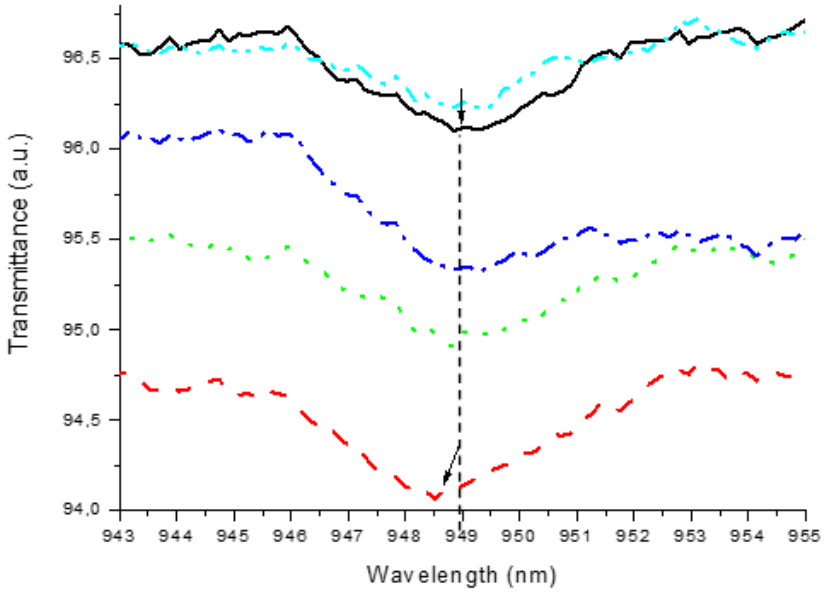

Figure 6. Localized Surface Plasmonic Resonance (LSPR) measurement: resonance and peak shift under laser pointer illumination; black line: initial curve; red curve: under illumination; green, blue: after switch-off; light blue: final configuration. λ = 405 nm; power ~25 mW; spot area = 1 cm^2.

These data on one side highlight the plasmonic properties of the realized nanostructure; on the other side, they point out the present limitations given by the weak resonance. The reason lies in the limited amount of gold that has been exfoliated and in the homogeneity of the created nanoholes. The improvement of these parameters is the goal of the forthcoming investigation on this subject.

As already mentioned, the location (949 nm) of the resonance shows a remarkable change with repect to the nanopillar structucture realized on an ITO substrate (633 nm). Additionally, under illumination, we observe a reduction of the overall transmittance, a slight change in the shape, and a small peak shift (approximately 0.5 nm), which goes back to the initial position when the laser pointer is switched off. Actually, this shift is of the same order of magnitude of the spectral sensitivity of the system; therefore, no definite statement can be done on this result, even if the reproducibility of this measurement is high, being observed many times.

Finally, the photomobility of the system is assessed by using a laser light to induce the motion of a PMP-metacrystal film having aperiodic dodecagonal symmetry. The effect is observed exploiting an optical microscope with objective 100×, N.A. 0.90, whose focal area is easily identified in the image pattern and is shown between the dashed white lines in Figure 7 (see also Video S1, Supporting Information). (The shape of the area in focus is determined by the non-uniform shape of the PMP film).

The focus area (Figure 7a) is shifted under illumination, due to PMP surface deformation (Figure 7b). When the light is switched off (Figure 7c,d), the PMP film restores its initial position in a few seconds (Figure 7d). It has to be remarked that the motion starts quickly under light illumination, while the restoring time (the time used to restore the initial position of the PMP film) corresponds to several seconds. The onset of light-induced actuation is consistent with the properties of the PMP film [16], whereas the restoring forces are probably due to the energy dissipation, depending on the thermal capacity and affecting the interfacial tension gradient of the biphasic PMP film inducing its bend, as described above. The motion at the micro-scale is also reasonably amplified by the plasmonic effect generated by the incident light (λ = 785 nm light, approximately 3 mW on the sample). In fact, motion is not recorded when illuminating regions with gold on the surface but away from the nano-patterned structure, thus confirming the plasmonic role in the observed PMP mobility.

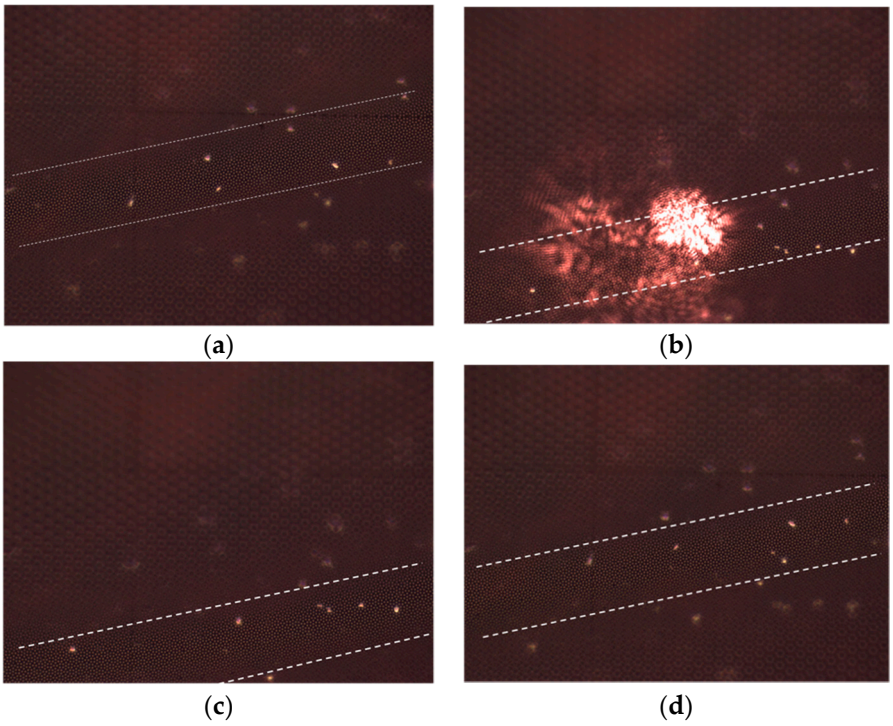

Figure 7. Dark field microscopy analysis of the laser-light-induced motion of a dodecagonal symmetry plasmonic crystal nestled on the PMP film surface. The area in focus of the microscope objective is edged by dashed white lines. (**a**) light off: initial position; (**b**) light on: shift of the focus area under illumination (λ = 785 nm; power on sample approximately 3 mW); (**c**) light OFF: inertial motion after irradiation; (**d**) light OFF: restoring of the initial position.

4. Conclusions

We have discussed different approaches in PMP manufacturing focusing on a novel approach based on light-induced modulation of the surface tension at the polymer interface. We have shown that these materials are suitable to develop a novel method to modify the PMP properties in order to get a nano-patterned photomobile polymer with plasmonic properties. This is achieved by using a novel organic mixture that under photopolymerization allows obtaining sensitive PMPs and exfoliation of the nanostructures. The plasmonic properties are highlighted by the LSPR whose intensity decreases under illumination with a moderate power light source. The plasmonic-related motion of the polymer is also recorded.

Supplementary Materials: The following are available online at http://www.mdpi.com/2073-4352/10/8/660/s1, Video S1: Light-induced motion of Plasmonic PMP film.

Author Contributions: Conceptualization, R.C.; methodology, for nanostructured-PMP fabrication: R.C.; methodology for EBL nanopatterned substrates fabrication, M.R., L.P., R.C.; investigation, R.C., M.R., F.V.; data curation, R.C., M.R., F.V.; writing—original draft preparation, R.C.; writing—review and editing, R.C. and F.S.; supervision, F.S., L.P., G.N., R.C., M.R., F.V.; funding acquisition, L.P. All authors have read and agreed to the published version of the manuscript.

Funding: This research was founded by the European Union under the programme FET-OPEN within the project "PULSE-COM" grant agreement no. 863227.

Acknowledgments: Special thanks to JordankaTasseva of the National Institute of Nuclear Physics, Naples, Italy.

Conflicts of Interest: The authors declare no conflict of interest.

References

1. Okawa, D.; Pastine, S.J.; Zettl, A.; Fréchet, J.M.J. Surface Tension Mediated Conversion of Light to Work. *J. Am. Chem. Soc.* **2009**, *131*, 5396–5398. [CrossRef] [PubMed]
2. Yu, Y.; Nakano, M.; Ikeda, T. Directed bending of a polymer film by light. *Nature* **2003**, *425*, 145. [CrossRef] [PubMed]
3. Briand, D.; Yeatman, E.; Roundy, S. *Micro Energy Harvesting*; Wiley-VCH Verlag GmbH & Co. KGaA: Wheinheim, Germany, 2015.
4. Harrop, P.; Das, R. *Energy Harvesting and Storage for Electronic Devices 2009–2019*; IDTechEx Ltd.: Cambridge, UK, 2009.
5. Ikeda, T.; Ube, T. Photomobile polymer materials: From nano to macro. *Mater. Today* **2011**, *14*, 480–487. [CrossRef]
6. Marangoni, C. Sul principio della viscosita' superficiale dei liquidi stabilito dal Sig. J. Plateau. *Nuovo Cimento* **1871**, *5*, 239–273. [CrossRef]
7. Lucchetta, D.E.; Simoni, F.; Nucara, L.; Castagna, R. Controlled-motion of floating macro-objects induced by light. *AIP Adv.* **2015**, *5*, 77147. [CrossRef]
8. Lucchetta, D.E.; Simoni, F.; Nucara, L.; Castagna, R. Light Moves Macro-objects. *Prog. Electr. Res. Symp.* **2015**, *1486*, 113716.
9. Lucchetta, D.E.; Castagna, R.; Simoni, F. Light-actuated contactless macro motors exploiting Bénard–Marangoni convection. *Opt. Express* **2019**, *26*, 13574–13580. [CrossRef]
10. Maggi, C.; Saglimbeni, F.; Dipalo, M.; De Angelis, F.; Di Leonardo, R. Micromotors with asymmetric shape that efficiently convert light into work by thermocapillary effects. *Nat. Comm.* **2015**, *6*, 7855. [CrossRef]
11. Mallea, R.T.; Bolopion, A.; Beugnot, J.-C.; Lambert, P.; Gauthier, M. Laser-induced thermocapillary convective flows: A new approach for non-contact actuation at microscale at the fluid/gas interface. *IEEE/ASME Trans. Mechatron.* **2017**, *22*, 693–704. [CrossRef]
12. Hendarto, E.; Gianchandani, Y.B. Thermocapillary actuation of millimeter-scale rotary structures. *J. Microelectromech. Syst.* **2014**, *23*, 494–499. [CrossRef]
13. Angeloni, A.S.; Caretti, D.; Carlini, C.; Chiellini, E.; Galli, G.; Altomare, A.; Solaro, R.; Laus, M. Photochromic liquid-crystalline polymers. Main chain and side chain polymers containing azobenzene mesogens. *Liq. Cryst.* **1989**, *4*, 513–527. [CrossRef]
14. White, T.J.; Tabiryan, N.V.; Serak, S.V.; Hrozhyk, U.A.; Tondiglia, V.P.; Koerner, H.; Vaia, R.A.; Bunning, T.J. A high frequency photodriven polymer oscillator. *Soft Matter* **2008**, *4*, 1796–1798. [CrossRef]
15. Kondo, M.; Takemoto, M.; Fukae, R.; Kawatsuki, N. Photomobile Polymers from Commercially Available Compounds: Photoinduced Deformation of Side-Chain Polymers Containing Hydrogen-Bonded Photoreactive Compounds. *Polym. J.* **2012**, *44*, 410–414. [CrossRef]
16. Castagna, R.; Nucara, L.; Simoni, F.; Greci, L.; Rippa, M.; Petti, L.; Lucchetta, D.E. An Unconvetional Approach to Photomobile Composite Polymer Films. *Adv. Mater.* **2017**, *29*, 1604800. [CrossRef] [PubMed]
17. Pirani, F.; Angelini, A.; Frascella, F.; Rizzo, R.; Ricciardi, S.; Descrovi, E. Light-Driven Reversible Shaping of Individual Azopolymeric Micro-Pillars. *Sci. Rep.* **2016**, *6*, 31702. [CrossRef] [PubMed]
18. Pirani, F.; Angelini, A.; Frascella, F.; Descrovi, E. Reversible Shaping of Microwells by Polarized Light Irradiation. *Int. J. Polym. Sci.* **2017**, *6812619*, 1–5. [CrossRef]
19. Unser, S.; Bruzas, I.; He, J.; Sagle, L. Localized Surface Plasmon Resonance Biosensing: Current Challenges and Approaches. *Sensors* **2015**, *15*, 684–688. [CrossRef] [PubMed]
20. Bingham, J.M.; Hall, W.P.; Van Duyne, R.P. Exploring the Unique Characteristics of LSPR Biosensing. *Nanoplasmonic Sens.* **2012**, 29–58. [CrossRef]
21. Rippa, M.; Castagna, R.; Pannico, M.; Musto, P.; Tkachenko, V.; Zhou, J.; Petti, L. Engineered Plasmonic Thue-Morse Nanostructures for LSPR Detection of the Pesticide Thiram. *Nanophotonics* **2017**, *6*, 1083–1088. [CrossRef]
22. Zheng, J.; He, L. Surface-Enhanced Raman Spectroscopy for the Chemical Analysis of Food. *CRFSFS* **2014**, *13*, 317–321. [CrossRef]
23. Hughes, J.; Izake, E.L.; Lott, W.B.; Ayoko, G.A.; Sillence, M. Ultra Sensitive Label Free Surface Enhanced Raman Spectroscopy Method for the Detection of Biomolecules. *Talanta* **2014**, *130*, 20–25. [CrossRef] [PubMed]

24. Luo, S.-C.; Sivashanmugan, K.; Liao, J.-D.; Yao, C.-K.; Peng, H.-C. Nanofabricated SERS-Active Substrates for Single Molecule to Virus Detection in Vitro: A Review. *Biosens. Bioelectron.* **2014**, *61*, 232–235. [CrossRef] [PubMed]
25. Rippa, M.; Castagna, R.; Pannico, M.; Musto, P.; Bobeico, E.; Zhou, J.; Petti, L. Plasmonic Nanocavities-Based Aperiodic Crystal for Protein-Protein Recognition SERS Sensors. *Opt. Data Process. Storage* **2017**, *3*, 54–60. [CrossRef]
26. Rippa, M.; Castagna, R.; Pannico, M.; Musto, P.; Bobeico, E.; Zhou, J.; Petti, L. High-Performance Nanocavities-Based Meta-Crystals for Enhanced Plasmonic Sensing. *Opt. Data Process. Storage* **2016**, *2*, 22–29. [CrossRef]
27. Salomon, A.; Prior, Y.; Fedoruk, M.; Feldmann, J.; Kolkowski, R.; Zyss, J. Plasmonic coupling between metallic nanocavities. *J. Opt.* **2014**, *16*, 114012. [CrossRef]
28. Lee, K.-L.; Wu, T.-Y.; Hsu, H.-Y.; Yang, S.-Y.; Wei, P.-K. Low-Cost and Rapid Fabrication of Metallic Nanostructures for Sensitive Biosensors Using Hot-Embossing and Dielectric-Heating Nanoimprint Methods. *Sensors* **2017**, *17*, 1548. [CrossRef]
29. Aksu, S.; Huang, M.; Artar, A.; Yanik, A.A.; Selvarasah, S.; Dokmeci, M.R.; Altug, H. Flexible Plasmonics on Unconventional and Nonplanar Substrates. *Adv. Mater.* **2011**, *23*, 4422–4432. [CrossRef]
30. Kahraman, M.; Daggumati, P.; Kurtulus, O.; Seker, E.; Wachsmann-Hogiu, S. Fabrication and Characterization of Flexible and Tunable Plasmonic Nanostructures. *Sci. Rep.* **2013**, *3*, 3396. [CrossRef]
31. Childs, W.R.; Nuzzo, R.G. Decal Transfer Microlithography: A New Soft-Lithographic Patterning Method. *J. Am. Chem. Soc.* **2002**, *124*, 13583–13596. [CrossRef] [PubMed]
32. Henzie, J.; Lee, M.H.; Pryce, I.M.; Aydin, K.; Kelaita, Y.A.; Briggs, R.M.; Atwater, H.A. Highly Strained Compliant Optical Metamaterials with Large Frequency Tunability. *Nano Lett.* **2010**, *10*, 4222–4235.
33. Lee, M.H.; Huntington, M.D.; Zhou, W.; Yang, J.-C.; Odom, T.W. Programmable Soft Lithography: Solvent-Assisted Nanoscale Embossing. *Nano Lett.* **2010**, *11*, 311–320. [CrossRef] [PubMed]
34. Rippa, M.; Capasso, R.; Petti, L.; Nenna, G.; De Girolamo Del Mauro, A.; Maglione, M.G.; Minarini, C. Nanostructured PEDOT:PSS Film with Two-Dimensional Photonic Quasi Crystals for Efficient White OLED Devices. *J. Mater. Chem. C* **2015**, *3*, 147–152. [CrossRef]
35. Criante, L.; Vita, F.; Castagna, R.; Lucchetta, D.E.; Simoni, F. Characterization of Blue Sensitive Holographic Polymer Dispersed Liquid Crystal for Microholographic Data Storage. *Mol. Cryst. Liq. Cryst.* **2007**, *465*, 203–207. [CrossRef]
36. Criante, L.; Lucchetta, D.E.; Vita, F.; Castagna, R.; Simoni, F. Distributed feedback all-organic microlaser based on holographic polymer dispersed liquid crystals. *Appl. Phys. Lett.* **2009**, *94*, 111114. [CrossRef]
37. Vita, F.; Lucchetta, D.E.; Castagna, R.; Francescangeli, O.; Criante, L.; Simoni, F. Detailed investigation of high-resolution reflection gratings through angular-selectivity measurements. *J. Opt. Soc. Am. B* **2007**, *24*, 471–476. [CrossRef]
38. Venhoven, B.A.; De Gee, A.J.; Davidson, C.L. Polymerization contraction and conversion of light-curing BisGMA-based methacrylate resins. *Biomaterials* **1993**, *14*, 871–875. [CrossRef]
39. Peutzfeld, A. Resin Composites in Dentistry: The Monomer Systems. *Eur. J. Oral Sci.* **1997**, *105*, 97–116. [CrossRef]
40. Lucchetta, D.E.; Spegni, P.; Di Donato, A.; Simoni, F.; Castagna, R. Hybrid Surface-Relief/Volume One Dimensional Holographic Gratings. *Opt. Mater.* **2015**, *42*, 366–369. [CrossRef]
41. Qi, J.; Sousa, M.E.; Fontecchio, A.K.; Crawford, G.P. Temporally Multiplexed Holographic Polymer-Dispersed Liquid Crystals. *Appl. Phys. Lett.* **2003**, *82*, 1652–1654. [CrossRef]
42. Qi, J.; De Sarkar, M.; Warren, G.T.; Crawford, G.P. In situ shrinkage measurement of holographic polymer dispersed liquid crystals. *J. Appl. Phys.* **2002**, *91*, 4795–4800. [CrossRef]
43. Castagna, R.; Vita, F.; Lucchetta, D.E.; Criante, L.; Simoni, F. Superior Performance Polymeric Composite Materials for High Density Optical Data storage. *Adv. Mater.* **2009**, *21*, 589–592. [CrossRef]
44. Watts, D.C.; Hindi, A. Intrinsic 'Soft-Start' Polymerisation Shrinkage-Kinetics in an Acrylate-Based Resin-Composite. *Dent Mater.* **1999**, *15*, 39–45. [CrossRef]
45. Castagna, R.; Vita, F.; Lucchetta, D.E.; Criante, L.; Greci, L.; Ferraris, P.; Simoni, F. Nitroxide Radicals Reduce Shrinkage in Acrylate-Based Holographic Gratings. *Opt. Mater.* **2007**, *30*, 539–544. [CrossRef]

46. Ackam, N.; Crisp, J.; Holman, R.; Kakkar, S.; Kennedy, R. Shrinkage: Its Measurement and Consequences. *Radtech Eur.* **1995**, *71*. Available online: https://www.radtech-europe.com/knowledge-center/articles/other/shrinkage-its-measurement-and-consequences (accessed on 19 July 2020).
47. Heilmann, S.M.; Moon, J.D. Multiacrylate Cross-Linking Agents in Pressure-Sensitive Photoadhesives. U.S. Patent 4,379,201 A, 5 April 1983.
48. Lazear, N.R.; Stackman, R.W. Ultraviolet Initiator Systems for Pressure-Sensitive Adhesives. U.S. Patent 4,150,170 A, 17 April 1979.
49. Kaczmarek, H.; Decker, C. Interpenetrating Polymer Networks. I. Photopolymerization of Multiacrylate Systems. *J. Appl. Polym. Sci.* **1994**, *54*, 2147–2156. [CrossRef]
50. Tobing, S.D.; Klein, A. Molecular Parameters and their relation to the Adhesive Performance of Acrylic Pressure-Sensitive Adhesives. *J. Appl. Polym. Sci.* **2001**, *79*, 2230–2244. [CrossRef]
51. Pradeep, K.; Deshpande, D.A.; Babu, G.N. Pressure Sensitive Adhesives of Acrylic Polymers Containing Functional Monomers. *Polymer* **1982**, *23*, 937–939.
52. Dewaele, M.; Truffier-Boutry, D.; Leloup, G.; Devaux, J. Volume Contraction in Photocured Dental Resins: The Shrinkage-Conversion Relationship Revisited. *Dent. Mater.* **2006**, *22*, 359–365. [CrossRef] [PubMed]
53. Pappas, S.P. *Radiation Curing Science and Technology*; Plenum Press: New York, NY, USA, 1992.
54. Loshaeck, S.; Fox, T.G. Cross-linked Polymers. I. Factors Influencing the Efficiency of Cross-linking in Copolymers of Methyl Methacrylate and Glycol Dimethacrylates. *J. Am. Chem. Soc.* **1953**, *75*, 3544–3550. [CrossRef]

© 2020 by the authors. Licensee MDPI, Basel, Switzerland. This article is an open access article distributed under the terms and conditions of the Creative Commons Attribution (CC BY) license (http://creativecommons.org/licenses/by/4.0/).